Magnetic structure of the high-density single-valent e_g Jahn-Teller system $LaMn_7O_{12}$

Andrea Prodi,[1] Edi Gilioli,[1] Riccardo Cabassi,[1] Fulvio Bolzoni,[1] Francesca Licci,[1] Qingzhen Huang,[2] Jeff W. Lynn,[2] Marco Affronte,[3] Andrea Gauzzi,[4,*] and Massimo Marezio[1,5]

[1]*Istituto dei Materiali per Elettronica e Magnetismo del Consiglio Nazionale delle Ricerche, Area delle Scienze, 43100 Parma, Italy*

[2]*NIST Center for Neutron Research, Gaithersburg, Maryland 20899, USA*

[3]*CNR-INFM and Dipartimento di Fisica, Università di Modena e Reggio Emilia, 41100 Modena, Italy*

[4]*Institut de Minéralogie et de Physique des Milieux Condensés, Université Pierre et Marie Curie-Paris VI, CNRS, 75005 Paris, France*

[5]*CRETA CNRS, 38042 Grenoble cedex 9, France*

(Received 4 November 2008; revised manuscript received 9 January 2009; published 11 February 2009)

We studied the structural and physical properties of powder samples of the high-pressure $LaMn_7O_{12}$ compound by means of neutron diffraction, dc magnetization, specific-heat, and dc electrical resistivity measurements. Our structural refinement shows that $LaMn_7O_{12}$ is the counterpart with *quadruple* perovskite structure of the well-known simple-perovskite $LaMnO_3$ because both compounds are single-valent Mn^{3+} systems sharing a similar pseudocubic network of buckled corner-sharing MnO_6 octahedra distorted by the Jahn-Teller (JT) effect. Besides this similarity, $LaMn_7O_{12}$ exhibits the following structural differences: (i) a monoclinic $I2/m$, instead of orthorhombic *Pnma*, structure; (ii) a much larger buckling of the MnO_6 octahedra, corresponding to a Mn-O-Mn bond angle as small as $\psi=180°-\phi=136°$. At $T_{N,B}=78$ K, the neutron data show evidence of an antiferromagnetic (AFM) structure of the octahedral Mn^{3+} ions (B sites), which consists of ferromagnetically coupled antiferromagnetic *ac* planes. This structure, commonly referred to as *C* type, markedly differs from the *A*-type structure of $LaMnO_3$, which consists of *antiferromagnetically* coupled *ferromagnetic ac* planes. We argue that this difference may be due not only to the different buckling, because the magnetic superexchange interaction is sensitive to ϕ, but also to the existence of two distinct JT distorted B sites, a characteristic feature of the quadruple perovskite structure not found in $LaMnO_3$. A further feature of this structure is the presence of a pseudocubic sublattice of JT Mn^{3+} ions with square coordination (A' site) in addition to the B-site sublattice. At $T_{N,A'}=21$ K, the A' sublattice of $LaMn_7O_{12}$ is found to form a second AFM structure consisting of AFM coupled ferromagnetic planes. This additional ordering appears to occur independently of that of the B sublattice. Finally, we observed a thermally activated insulating behavior of the resistivity similar to that previously reported for $LaMnO_3$, which confirms the hypothesis that the superexchange interaction is predominant in single-valent systems while the double-exchange interaction is relevant only in mixed-valence or disordered systems.

DOI: 10.1103/PhysRevB.79.085105 PACS number(s): 71.70.Ej, 61.66.Fn, 75.25.+z, 75.30.−m

I. INTRODUCTION

As first reported by Wollan and Koehler,[1] manganese oxides with perovskitelike structure, such as the prototype $La_{1-x}Sr_xMnO_3$ system, display a rich variety of competing charge, spin, and orbital orderings of the Mn^{3+} or Mn^{4+} ions.[2] The stability of these orderings is controlled by the relative proportion of the two ions and by temperature, pressure, and magnetic field, which leads to remarkable properties, such as the colossal magnetoresistance.[3] In order to provide a theoretical account of the various orderings found experimentally, Goodenough[4] showed the dominant role of the Anderson superexchange interaction[5] between neighboring Mn ions through the Mn-O-Mn path of the corner-sharing network of MnO_6 octahedra. The Goodenough-Kanamori-Anderson (GKA) rules[4,6,7] provide a general—although simplified—frame for describing the strength and sign of the magnetic interaction and the Jahn-Teller (JT) driven polarization of the two relevant e_g $d_{x^2-y^2}$ or $d_{3z^2-r^2}$ orbitals in the MnO_6 octahedra. In this respect, the key parameters are the Mn-O-Mn bond angle, ψ, and the Mn-O bond length. It follows that the stabilization of given charge, magnetic, and orbital orderings requires a well-defined pattern of cooperative buckling and distortion of the octahedral network.

In this work, we address the question of the validity of the above ordering models for other e_g systems sharing a similar perovskitelike network but with a different crystal symmetry. We should restrict ourselves to single-valent systems, where only Mn^{3+} ions are present; thus only magnetic and orbital orderings are to be considered. At low temperatures, the compounds of the perovskitelike $RMnO_3$ system (R=La or other trivalent rare earths) develop a characteristic antiferromagnetic (AFM) ordering of the octahedral Mn^{3+} ions of the pseudocubic B-site sublattice.[1] This ordering consists of antiferromagnetically coupled ferromagnetic (FM) planes, which is commonly known as *A*-type structure, according to the classification proposed by Bertaut.[8] In the $RMnO_3$ system, this AFM order is stabilized within an orthorhombic *Pnma* structure of $GdFeO_3$ type.[1,9,10] The orthorhombic distortion of the pristine cubic structure is in agreement with the GKA rules. The key role played by the octahedral buckling in stabilizing this magnetic structure is evident considering that the ordering (Néel) temperature, T_N, scales with the bending angle, $\phi=180°-\psi$, as $\langle\cos^2\phi\rangle$.[11]

As a counterpart of the prototype $RMnO_3$ system, here we consider the single-valent system $LaMn_7O_{12}$ characterized by a *quadruple* perovskite structure first proposed by Marezio *et al.*[12] for $NaMn_7O_{12}$ in 1973 and shortly after reported in the series of AMn_7O_{12} compounds, with

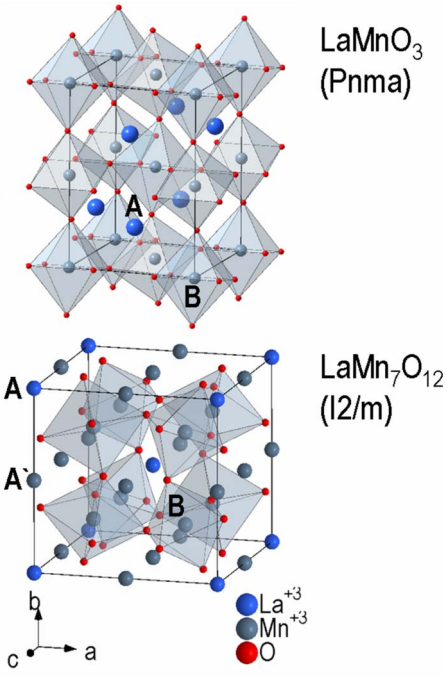

FIG. 1. (Color online) Nuclear structure of $LaMn_7O_{12}$ (right) as compared to $LaMnO_3$ (left). Note in the former the two crystallographically distinct Mn^{3+} sites with octahedral (B-site) and square-planar (A'-site) coordinations, and the larger buckling of the MnO_6 octahedra.

A=Ca,Cd,Sr,La,Nd.[13] An isostructural compound $CaCu_3Ti_4O_{12}$ was actually synthesized by Deschanvres *et al.*[14] earlier in 1967 but the detailed structure was not reported. As shown below, $LaMn_7O_{12}$ shares with $LaMnO_3$ and related compounds the same single-valent e_g Mn^{3+} characteristic and a similar pseudocubic network of buckled MnO_6 octahedra (see Fig. 1). The main point of this work is that, in spite of these similarities, the octahedral Mn^{3+} ions of $LaMn_7O_{12}$ develop an unusual magnetic C-type structure, which consists of ferromagnetically coupled antiferromagnetic planes. Our analysis suggests that this fundamental difference can be explained by taking into account the following structural characteristics of the quadruple perosvkite structure: (i) the larger buckling of the MnO_6 octahedra and (ii) the existence of two, instead of just one, distinct JT distorted octahedral Mn^{3+} B sites. This points at the primary importance of crystal symmetry in controlling the stability of competing magnetic and orbital orderings in perovskitelike e_g systems. Thus, $LaMn_7O_{12}$ appears to be a model system for generalizing the GKA rules to a wider range of superexchange parameters and to explore the stability conditions of unusual magnetic and orbital orderings by using crystal symmetry as additional control parameter.

The paper is organized as follows. In Sec. II, we report on the synthesis method employed to obtain single-phase powder samples and single crystals of $LaMn_7O_{12}$. In Sec. III A we report and discuss the structural properties of $LaMn_7O_{12}$ obtained from powder neutron and x-ray diffractions. In Sec. III B we illustrate the magnetic, thermodynamic, and transport properties. Finally, in Sec. IV we discuss the results with emphasis on the peculiar properties of the magnetic ground state as compared to $LaMnO_3$.

II. EXPERIMENTAL

A. Synthesis

$LaMn_7O_{12}$ was synthesized under high pressure at P =4 GPa and T=1000 °C using either a multianvil press or a conventional piston-cylinder one. Synthesis times of 1–2 h led to the formation of powder samples while longer (≈10 h) times enabled the formation of ≈300 μm single crystals. Attempts to obtain the compound at lower pressure and temperature using the hydrothermal synthesis route, as in the case of the isostructural $ACu_3Mn_4O_{12}$ system, with A =La, Lu, or Y,[15] were not successful. The volume variation between the competing $LaMnO_3$ and Mn_2O_3 phases, and the quenched $LaMn_7O_{12}$ phase is as large as ≈−4.8% at 1 atm.[13] This explains the importance of high-pressure techniques to stabilize the $LaMn_7O_{12}$ phase and confirms its feature to be a high-density compound. Powder x-ray diffraction analysis using a laboratory Cu K_α diffractometer in the Bragg-Brentano geometry confirms the purity of the as-prepared powder to be above 95% and no traces of the aforementioned competing phases were found.

Neutron powder-diffraction experiments were carried out at the NIST Center for Neutron Research in Gaithersburg. A preliminary study was performed at the high-intensity low-resolution BT7 beamline using a double crystal pyrolithic graphite (200) monochromator used to select a neutron wavelength of 2.4701 Å. This study enabled us to identify the magnetic peaks by comparing three spectra taken at 7, 110, and 220 K. Subsequently, various spectra were taken as a function of temperature in the 300–3.5 K range using the high-resolution BT1 and BT2 instruments. These are equipped with Cu(311) and Ge(311) monochromators used to select neutron wavelengths of 1.5402 and 2.0775 Å, respectively. These two wavelengths are optimized for an accurate determination of the nuclear and magnetic structures, respectively. Intensities were collected for 6 h at each temperature using a ≈1 g powder sample. The structural refinements of both nuclear and magnetic structures were performed using the GSAS software package.[16]

Temperature-dependent specific heat, C, magnetization, M, and dc electrical resistivity, ϱ, were measured in both zero-field-cooling (ZFC) and field-cooling (FC) modes at various fields using a commercial quantum design physical property measurement system (PPMS) and a commercial quantum design superconducting quantum interference device (SQUID) magnetometer equipped with 7 and 5.5 T superconducting magnets, respectively. The specific heat was measured from 2 to 300 K using a standard 2τ method. The dc electrical resistivity was measured in the standard van der Pauw configuration in the 300–170 K range. At lower temperatures, the measurement was not possible because the sample resistance increased beyond the operating range of the voltmeter.

III. RESULTS

A. Structural properties

1. Neutron powder diffraction

In agreement with the report by Bochu *et al.*,[13] our neutron-diffraction data for $LaMn_7O_{12}$ were successfully re-

TABLE I. Rietveld refinement of the $LaMn_7O_{12}$ structure within the $I2/m$ space group (Ref. 18) obtained from the powder neutron-diffraction data at 300 and 10 K. The values in Å of the thermal U factors are multiplied by 100. Numbers in parentheses indicate statistical uncertainty.

Temperature	300 K	10 K
a,b,c(Å)	7.50909(15), 7.37391(12), 7.50070(15)	7.50876(19), 7.34893(16), 7.50374(19)
β(°)	91.228(1)	91.354(2)
V(Å)^3	415.23(5)	413.95(3)
	La $2a$ (0,0,0)	
U_{iso}	0.78(9)	1.21(20)
	Mn1 $2b(0,1/2,0)$, $2c(1/2,0,0)$, $2d(1/2,1/2,0)$	
U_{iso}	1.12(9)	1.21(5)
	Mn2 $4e(1/4,1/4,1/4)$, $4f(1/4,1/4,3/4)$	
U_{iso}	0.37(7)	0.15(15)
	O1 $4i(x,0,z)$	
x,z	0.1680(5), 0.3070(5)	0.1693(10), 0.3087(10)
U_{11}, U_{22}, U_{33}	1.01(25), 0.12(19), 0.66(23)	
U_{12}, U_{13}, U_{23}	0, −0.78(17), 0	
U_{iso}		0.98(18)
	O2 $4i(x,0,z)$	
x,z	0.1804(7), 0.6862(6)	0.1783(10), 0.6875(11)
U_{11}, U_{22}, U_{33}	1.50(27), −0.19(18), 1.64(26)	
U_{12}, U_{13}, U_{23}	0, −0.97(19), 0	
U_{iso}		1.04(20)
	O3 $8j(x,y,z)$	
x,y,z	0.0154(5), 0.3119(5), 0.1711(5)	0.0164(7), 0.3131(8), 0.1735(7)
U_{11}, U_{22}, U_{33}	1.34(20), 0.52(16), 1.76(20)	
U_{12}, U_{13}, U_{23}	0.13(13), −1.11(20), 0.37(13)	
U_{iso}		0.62(19)
	O4 $8j(x,y,z)$	
x,y,z	0.3129(4), 0.1768(5), −0.0127(4)	0.3134(7), 0.1757(9), −0.0132(7)
U_{11}, U_{22}, U_{33}	1.26(19), 0.39(18), 0.79(20)	
U_{12}, U_{13}, U_{23}	0.20(12), −0.61(18), −0.06(14)	
U_{iso}		0.95(20)
wR_p, R_p, χ^2 (%)	0.0534, 0.0428, 0.8254	0.0862, 0.0670, 0.94
No. of free param.	80	47

fined in the monoclinic $I2/m$ space group in the whole 3.5–300 K range studied. The room-temperature unit-cell parameters were found to be $a=7.50909(14)$, $b=7.37391(12)$, $c=7.50070(15)$ Å, and $\beta=91.228(1)°$. This is a pseudocubic perovskitelike structure which belongs to the family of *quadruple* perovskites of general formula $AA'_3B_4O_{12}$, where A is a nonmagnetic monovalent, divalent, or three-valent cation, and A' and B are JT ions. In the case of $LaMn_7O_{12}$, both A' and B sites are occupied by Mn^{3+} ions. The simplified unit cell (see Fig. 1) is obtained by doubling the unit cell of the simple-perovskite ABO_3 along the three pseudocubic crystallographic axes (note that, in $LaMn_7O_{12}$, $a\approx b\approx c\approx 2a_p$, where a_p is the lattice parameter of the ideal cubic perovskite). The resulting $I2/m$ body-centered pseudocubic unit cell is characterized by two interpenetrating sublattices of JT ions with octahedral (B site) and square-planar (A' site) coordinations while the A (La^{3+} in our case) ion occupies the icosahedral (0,0,0) position. From Fig. 1 it is noted that, in the cubic cell which approximately describes the monoclinic cell, the eight B ions occupy the $(\frac{1}{4},\frac{1}{4},\frac{1}{4})$ and equivalent positions. The monoclinic distortion splits this pristine eightfold site into two fourfold $4e$ and $4f$ sites, and the resulting site symmetry is lowered from mmm to $\bar{1}$. The symmetry lowering leads to a similar splitting of the pristine sixfold A' site into three twofold sites with $2/m$ point symmetry. Such situation of distinct Mn B sites is not found in the simple-perovskite compound $LaMnO_3$, where all the Mn^{3+} (B) sites occupy the $4a$ sites of the $Pnma$ symmetry.[1,9,10]

The entire list of the refined structural parameters at two representative temperatures of 300 and 10 K are reported in Table I. The Mn-O bond distances obtained from the refinement are reported in Table II for the two $4e$ and $4f$ octahedral sites. A bond valence sum (BVS) analysis of these sites yields very similar values of 3.215 and 3.178, respectively.

TABLE II. Selected distances in Å and bond angles in degrees for $LaMn_7O_{12}$ at 300 and 10 K obtained from the data of Table I. Numbers in parentheses indicate statistical uncertainty.

Temperature	300 K	10 K
Mn-O bond length (Mn *B* sites)		
Mn2(4*e*)-O1	1.993(2)	1.987(3)
Mn2(4*e*)-O3	1.901(4)	1.890(6)
Mn2(4*e*)-O4	2.107(3)	2.112(5)
Mn2(4*f*)-O2	1.972(2)	1.968(3)
Mn2(4*f*)-O3	2.141(4)	2.145(5)
Mn2(4*f*)-O4	1.909(3)	1.906(5)
Mn-O-Mn bond angles (Mn *B* sites)		
Mn2(4*e*)-O1-Mn(4*e*)	135.4(2)	135.2(4)
Mn2(4*f*)-O2-Mn(4*f*)	138.4(3)	138.0(5)
Mn2(4*e*)-O3-Mn(4*f*)	136.4(2)	136.9(3)

Taking into account the limited accuracy of the BVS analysis and its semiempirical meaning, we can conclude that no charge transfer across the two Mn 4*e* and 4*f* *B* sites occurs. The same conclusion applies to the three A' sites, for which the BVS analysis yields the values of 2.887, 3.077, and 2.824. In conclusion, the average BVS of all the Mn ions is 3.082, which corroborates our hypothesis that $LaMn_7O_{12}$ is a single-valent Mn^{3+} system.

In what follows, we discuss the two relevant structural features of $LaMn_7O_{12}$. (i) As expected from the previous symmetry considerations, the two 4*e* and 4*f* octahedral sites allow two different JT distortions of the MnO_6 octahedra. As noted in Tables I and II, and Fig. 3, the two sites do indeed display different Mn-O bond lengths corresponding to slightly different bond-length averages $\langle \text{Mn-O} \rangle_{4e}$ and $\langle \text{Mn-O} \rangle_{4f}$. At room temperature, the bond lengths of the 4*e* sites are 1.901(4), 1.993(2), and 2.107(3) Å [$\langle \text{Mn-O} \rangle_{4e}$ =2.000(3) Å] while those of the 4*f* sites are 1.909(3), 1.972(2), and 2.141(4) Å [$\langle \text{Mn-O} \rangle_{4f}$=2.007(3) Å]. From Fig. 3, one notes that these lengths do not vary significantly with temperature. In agreement with previous theoretical studies,[17,19] the above two distinct JT distortions are expected to lead to distinct superexchange interactions with the neighboring Mn sites, which is one of the main points of this work. (ii) Although $LaMn_7O_{12}$ exhibits an octahedral distortion pattern similar to that of $LaMnO_3$, the octahedral buckling of $LaMn_7O_{12}$ (and of all isostructural compounds with quadruple perovskite structure) turns out to be much larger owing to the Jahn-Teller distortion of the A' site. Specifically, the average Mn(*B*)-O-Mn(*B*) bond angle is $\psi=180° - \phi=136°$, compared to the average 155° value found in $LaMnO_3$.[9,10]

Finally, we would like to comment on the temperature-dependent changes in the nuclear structure. As mentioned above, no space-group changes are observed upon cooling down to 3.5 K. The temperature dependence of the unit-cell parameters reported in Fig. 2 shows that the monoclinic distortion increases upon cooling. Specifically, the *a* and *c* parameters are nearly unchanged while the *b* parameter along the twofold axis shrinks and the monoclinic angle β increases. At 78 K, one also notes a sudden increase in the slope of the temperature dependence of β concomitant to the AFM ordering of the *B* sublattice to be discussed below. This shows the existence of a coupling between the electronic energy associated with the magnetic ground state and the elastic energy. On the other hand, the octahedral Mn-O distances remain nearly constant within the experimental error (see Fig. 3). It follows that the shrinking of the cell upon cooling is due to a closer packing of the octahedra achieved through their rigid buckling around an axis perpendicular to *b*.

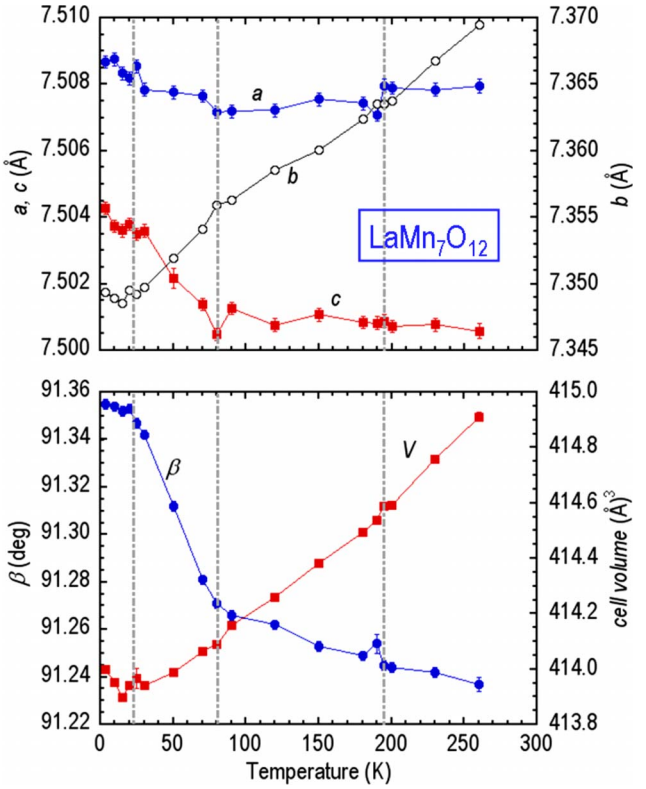

FIG. 2. (Color online) Lattice parameters and unit-cell volume, *V*, of $LaMn_7O_{12}$ as a function of temperature. Broken lines mark the onset of the magnetic orderings of the A' and *B* Mn sublattices at $T_{N,A'}=21$ K and $T_{N,B}=78$ K, respectively, and a structural anomaly at about 200 K, possibly associated with the presence of small amounts of $LaMnO_3$ impurities, as discussed in the text.

2. *Magnetic structure*

The most relevant structural changes occurring with decreasing temperature consist in the appearance of two magnetic orderings at low temperature. The magnetic contribution to the diffraction pattern was obtained after subtraction of the nuclear pattern. At low-temperature five magnetic peaks were detected, as shown by the low-resolution spectrum taken at 7 K (see Fig. 4). The (110), (211), and (220) peaks contribute to the nuclear Bragg peaks while the (100) and (201) ones are purely magnetic, as they are not allowed by the symmetry of the nuclear structure, which is the signature of an AFM long-range order. In Fig. 5, we show the temperature evolution of the magnetic moments obtained

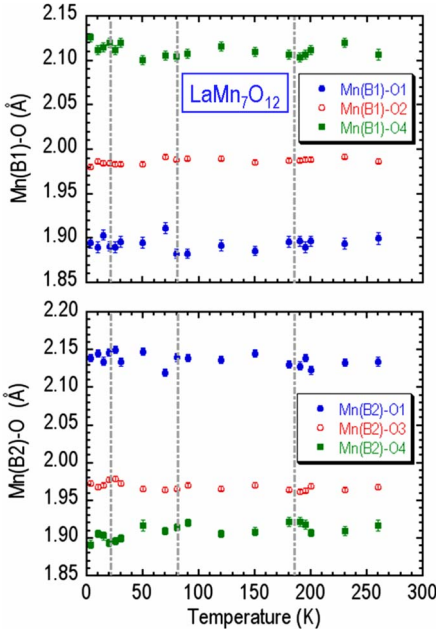

FIG. 3. (Color online) Mn-O bond distances as a function of temperature for the (a) 4*e* and (b) 4*f* octahedral sites. The vertical broken lines are as in the previous figure.

from the integrated intensities of the (110) and (201) peaks of the high-resolution spectra. The data analysis unveil two AFM orderings at $T_{N,B}$=78 K and $T_{N,A'}$=21 K associated with the (110) and (201) reflections, respectively. Similarly to the case of the isostructural compound $NaMn_7O_{12}$,[20] our symmetry analysis enables us to assign these two order parameters to the ordering of the *B* and $A'Mn^{3+}$ sublattices, respectively. Note that no anomalous behavior of the unit-cell parameters is found at the onset of the second transition, which indicates that the two orderings occur independently, as reported previously for $NaMn_7O_{12}$.[21]

A structural refinement of the magnetic structure using the high-resolution data taken at 3.5 K was performed by imposing equal *x* and *z* components of the magnetic moment, **M**, of both *B* and *A'* Mn ions because the *ac* plane is nearly squared. The results of the refinement are reported in Table

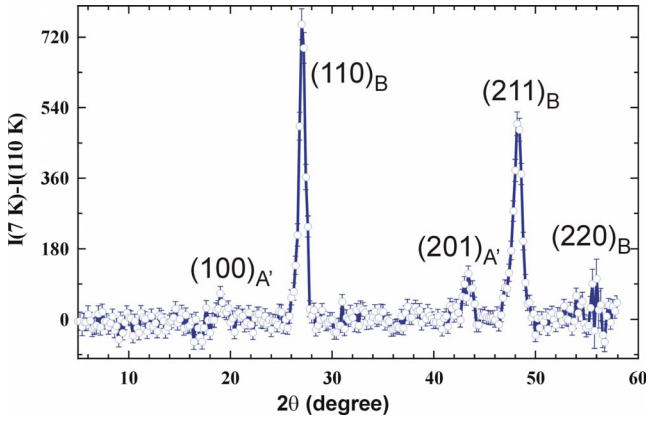

FIG. 4. (Color online) Magnetic Bragg peaks of $LaMn_7O_{12}$ measured at 7 K using a neutron wavelength of 2.4701 Å. The *A'* and *B* labels refer to the sublattice the peaks are associated to.

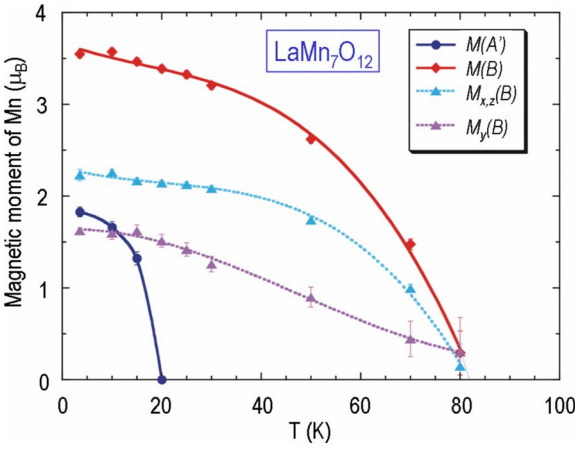

FIG. 5. (Color online) Temperature dependence of the Cartesian components and of the moduli of the moments for the two magnetic structures of the *A'* and *B* sublattices obtained from the refinement of the high-resolution neutron data taken using a wavelength of 2.0775 Å.

III. The magnetic structure of the *B* sublattice turns out to be of the *C* type [see Fig. 6(a)]. The refinement shows a good agreement between experimental and calculated magnetic peaks, and yields a moment value of $3.54(4)\mu_B$, somehow lower than the value of $4.0\mu_B$ expected for the high spin state (S=2) of Mn^{3+} ions. This confirms the inadequacy of a purely ionic description of the Mn^{3+} electronic states consistently with the well-known role of semicovalent magnetic exchange in perovskitelike manganese oxides.

In the following we should attempt to provide an account for the stability of the *C*-type magnetic structure of the *B* sublattice. We first note that the symmetry of the two inequivalent 4*e* and 4*f* *B* sites does indeed allow the two antiferromagnetically coupled ferromagnetic sublattices to form the *C*-type structure [see Fig. 6(a)]. In this structure all magnetic ions have two ferromagnetic and four antiferromagnetic nearest neighbors; hence the body-centered structure, the twofold axis, and the mirror plane characteristic of the nuclear structure are preserved and the resulting magnetic symmetry is described by the magnetic space group $I2'/m'$ (n° 62 in the Shubnikov notation). On the other hand, the *A*-type structure found in $LaMnO_3$ would not be compatible with this symmetry for the *A* structure consists of AFM coupled FM planes. Opposite conclusion is drawn by applying similar symmetry considerations to $LaMnO_3$ because the nuclear structure of this compound is primitive (*Pnma*) and the Mn *B* sites are all equivalent. It is therefore evident that the two magnetic structures found in $LaMn_7O_{12}$ and in $LaMnO_3$ reflect the different symmetry of their crystal structures. This shows that crystal symmetry can control the stability of competing magnetic structures in single-valent manganese oxides with perovskitelike structure. This conclusion constitutes one of the main points of our work.

We now consider the magnetic structure of the Mn^{3+} *A'* sublattice. The topology of this sublattice differs from that of the *B* sublattice, as seen from Figs. 1 and 6. The nearest neighbors of each *A'* ion are four, instead of six, and form a square within the plane of the ion, instead of an octahedron.

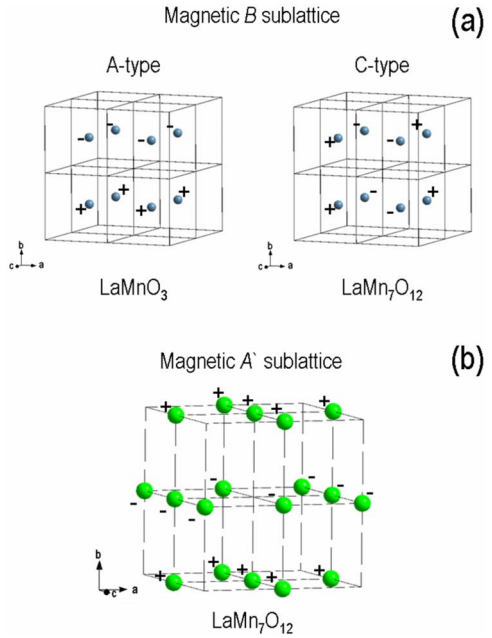

FIG. 6. (Color online) The magnetic structure of $LaMn_7O_{12}$ as determined from the neutron data. (a) The *C*-type AFM structure of the octahedral Mn(*B*) ions. The ions labeled as (−) and (+) indicate the 4*e* and 4*f* sites of the $I2/m$ space group (Ref. 18), respectively. The *A*-type structure of $LaMnO_3$ and related compounds is also shown for comparison. In this case, both types of (−) and (+) ions occupy the 4*a* sites of the *Pnma* space group. Note that the simplified magnetic *B* sublattice is simple cubic for both compounds. (b) The AFM structure of the square-planar coordinated Mn(A') ions.

The proposed AFM structure consistent with the neutron data is shown in Fig. 6(b). This structure consists of FM *ac* planes AFM coupled along the *b* axis, similarly to the *A* structure of the *B* sublattice found in $LaMnO_3$. In the refinement, the moment was set parallel to the *c* axis taking into account the symmetry and the stability of this configuration as compared to the perpendicular configuration. Under this constraint, the refinement yields a moment value of $1.82(5)\mu_B$ at 3.5 K, smaller than that of the Mn^{3+} *B* sublattice. This suggests that the electronic state describing the e_g electrons of the A' sites is different from that of the *B* sites. Specifically, the covalent character of the Mn-O bonds appears to be stronger for the A' sites. Owing to the limited number of magnetic peaks observed, the accurate determination of the magnitude and orientation of the ordered moments may require additional studies on large single crystals.

B. Physical properties

1. Specific heat

The specific heat as a function of temperature is reported in Fig. 7. The two anomalies at 78 and 21 K confirm the magnetic ordering transitions of the *B* and A' sublattices detected by neutron diffraction. The anomalies appear as smeared jumps, thus indicating that both phase transitions are of second order. The anomaly at 21 K is less pronounced and broadened over a 10 K range. This is consistent with the relative weakness of the magnetic peaks associated with the A' sublattice and the lower value of the effective moment. The lattice heat capacity could not be described by a single Debye formula in the whole temperature range. This may be due to the change in lattice dynamics induced by the magnetic transitions. At low temperature, the C/T data display the characteristic linear dependence with T^2 arising from the contribution of acoustic phonons. In the intermediate 15–100 K range, i.e., outside the range of validity of both high-temperature and low-temperature approximations, a reliable subtraction of the lattice contribution is not possible due to the lack of nonmagnetic isostructural compounds. Therefore, it appears difficult to estimate the entropy reduction at the magnetic transitions. In the high-temperature range, a Debye fit yields a Debye temperature as high as $\Theta_D=665$ K and a Sommerfeld coefficient $\gamma=12.45$ mJ/mol K^2. Both values turn out to be comparable with those previously reported for the isostructural compound $NaMn_7O_{12}$. It is truly exceptional to find such a large γ for an insulator (see Sec. III B 3 below) considering that, within a conventional Fermi-liquid theory, γ is proportional to the density of states and to the effective mass of the carriers. The interpretation of this puzzling aspect goes beyond the scope of this work. Also, the lattice contribution above 140 K is similar to that observed in $NaMn_7O_{12}$,[22] which also displays a high Θ_D value and a slow saturation of the $C(T)$ curve to the classical Dulong-Petit value.

2. dc magnetization

In Fig. 8, we report the ZFC and FC temperature-dependent magnetization curves, $M(T)$, for a polycrystalline sample measured in fields of 10 and 100 Oe. The two magnetic transitions seen in the $M(T)$ curves are in agreement with the ordering of the *B* and A' sublattices shown by the neutron data. The curves also display a minor transition at $T\simeq 200$ K of magnitude $\approx 2\times 10^{-3}$ of the total signal and is not visible in the scale of Fig. 8. This feature corresponds to the anomaly in the temperature dependence of the unit-cell

TABLE III. Refined magnetic moments in both Cartesian and spherical coordinates for the *B* and A' sublattices of $LaMn_7O_{12}$ obtained from the 3.5 K neutron-diffraction data. ϑ and φ indicate the colatitude and azimuthal angles, respectively. Moment and angle values are given in Bohr magneton units and degrees, respectively. Numbers in parentheses indicate statistical uncertainty.

Site	(x,y,z)	M_x	M_y	M_z	M	ϑ	φ
Mn(*B*)	(1/4,1/4,1/4)	2.225(31)	1.628(64)	−2.225(31)	3.543(42)	128.90(44)	36.20(1.23)
Mn(A')	(1/2,0,0)	0	0	1.821(56)	1.821(56)	0	0

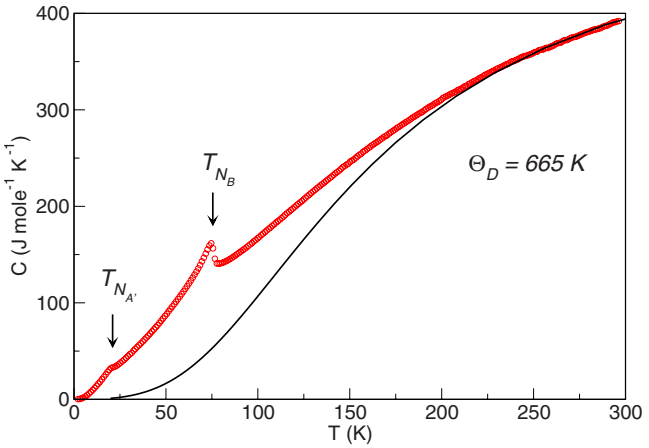

FIG. 7. (Color online) Specific heat of $LaMn_7O_{12}$. The solid line is a Debye fit in the high-temperature range.

parameters of Fig. 2. The anomaly may be ascribed to the presence of $LaMnO_3$ impurities, not detected either by x-ray or neutron diffraction, considering that the magnetic ordering in $LaMnO_3$ is known to occur in the same temperature range and to be sensitive to the oxygen content.[23,24] As expected from the neutron data, above $T_{N,B}$ the $M(T)$ curve displays a paramagneticlike behavior. Above 200 K, the data are well described by a classic Curie-Weiss law with a Weiss constant $\Theta_W = -47.84$ K, which supports the model of an AFM exchange between Mn ions, and an effective moment $\mu_{\text{eff}} = 4.78\mu_B$. The latter value is close to the theoretical value of $4.9\mu_B$ expected for a system of $N = N_{A'} + N_B$ spins with $S = 2$, which further supports the picture of single-valent Mn^{3+} system.

The signature of the magnetic orderings of the B and A' sublattices in the $M(T)$ curves is as follows. At $T_{N,A'}$ the $M(T)$ curve displays an AFM-like cusp, in agreement with the evidence of AFM ordering of the A' sublattice provided by the neutron data. On the other hand, at the ordering temperature of the B sublattice, $T_{N,B}$, the FC curve displays an FM-like response. At first glance, this response may appear to be inconsistent with the aforementioned AFM C-type structure. In fact, although our dc magnetization data on

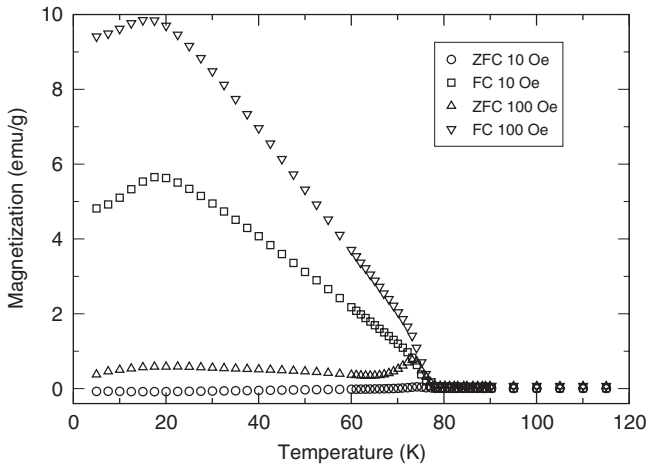

FIG. 8. FC and ZFC magnetizations of $LaMn_7O_{12}$ powders.

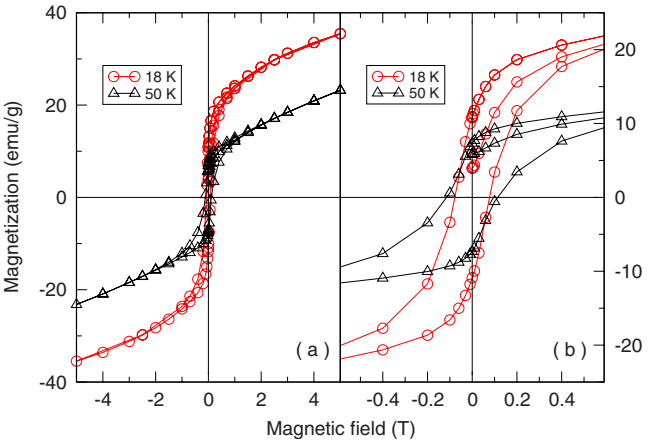

FIG. 9. (Color online) Magnetic hysteresis in $LaMn_7O_{12}$ at selected temperatures. (a) Full measurement range. (b) Expanded view of the low-field region.

polycrystalline samples do not allow differentiating of the distinct contributions of the two magnetic sublattices, this apparent inconsistency is explained by the following canting model. The model is supported by the previous neutron-diffraction data and by the behavior of hysteresis curves taken separately below $T_{N,B}$ and below $T_{N,A'}$ (see Fig. 9). The two hysteresis loops are qualitatively similar, with coercitive fields of $H_c \simeq 1150$ and 750 Oe at 50 and 18 K, respectively (the difference in H_c values can be explained by different domain-wall configurations). This similarity suggests that the hysteresis is not affected by the ordering of the A' spins. Hence, the weak ferromagnetism seen in the hysteresis curves cannot be ascribed either to an FM exchange coupling between the B and A' ions or to a spin canting induced by the competition of the magnetocrystalline anisotropy of the two B and A' sublattices. The field dependence of the loops rather suggests that the magnetic response is the sum of a first component with an extrinsic hysteretic regime at low fields and of a second one with a linear regime at high field characteristic of antiferromagnets.

Typically, a canting of an otherwise collinear spin structure is known to arise from the Dzyaloshinsky-Moriya (DM) interaction[25,26] between the spin-up and spin-down sublattices in the AFM structure or from a sizable single-ion anisotropy.[27] In what follows we should analyze the relevance of each of the two mechanisms. We first recall that the latter mechanism, often referred to as *magnetocrystalline anisotropy*, consists of the spin-orbit interaction between a magnetic ion whose orbital state is quenched and the crystal lattice. Thus, the magnetic energy depends upon the relative orientation of the magnetization with respect to the crystalline axes. On the other hand, the DM interaction is an antisymmetric spin-exchange interaction between two spins $\mathbf{S_i}$ and $\mathbf{S_j}$ described by the mixed product of the form $\mathcal{D}\cdot(\mathbf{S_i} \times \mathbf{S_j})$. It appears that this interaction can give rise to a weak ferromagnetic moment if the $\mathcal{D}$ vector has a nonzero component perpendicular to the plane of the two spins, which is indeed the case of the octahedral Mn ions in a buckled perovskitelike structure. A previous study[28] suggested that both mechanisms are necessary to account for the weak ferromag-

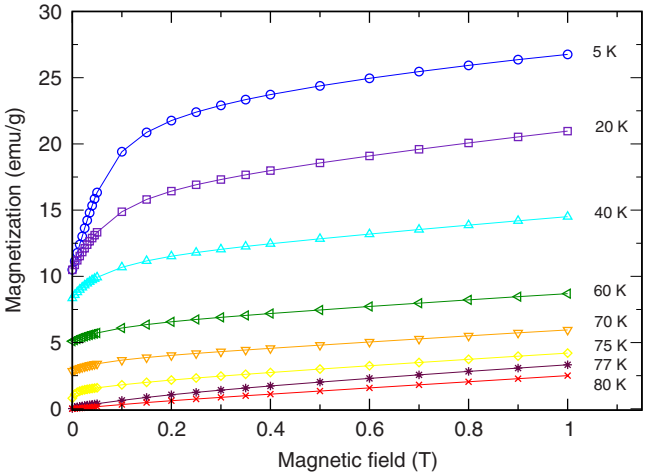

FIG. 10. (Color online) First magnetization $M(H)$ curves of $LaMn_7O_{12}$ obtained following the procedure described in the text.

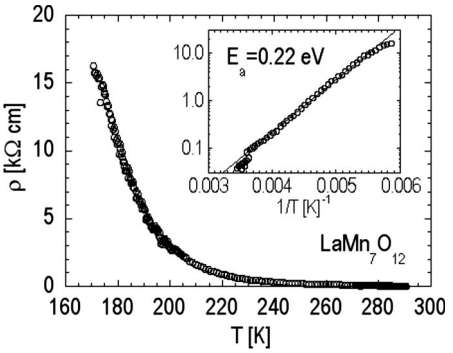

FIG. 11. Temperature dependence of the dc electrical resistivity of $LaMn_7O_{12}$. Inset: Arrhenius plot showing evidence of the thermally activated behavior of the charge carriers. The solid line is a linear data fit.

netism observed in $LaMnO_3$ single crystals and also for this compound a canted AFM structure with $0.18\mu_B$/Mn ion was proposed.

In $LaMn_7O_{12}$, the magnetic remanence of the B sublattice may be assessed by extrapolating down to zero field a hysteresis loop measured at an intermediate temperature between $T_{N,B}$ and $T_{N,A'}$, at which the magnetization of the A' sublattice is negligible while the magnetization of the B sublattice is nearly saturated. The loops measured at 50 and 40 K in Figs. 9 and 10, respectively, yield the same estimate for the ferromagnetic component of the B sublattice of about 10 emu/g, which indicates that the saturation condition is fulfilled for the B sublattice. The above value of magnetic remanence corresponds to $0.3\mu_B$/Mn ion, roughly twice that reported for $LaMnO_3$.[28] Taking into account that the DM remanence in polycrystalline samples typically is half that in single crystals and proportional to the magnitude of the $\mathcal{D}$ vector,[29] we estimate that $\mathcal{D}$ is four times larger in $LaMn_7O_{12}$ than in $LaMnO_3$. This estimate is consistent with the fact that the octahedral buckling is much larger in $LaMn_7O_{12}$. It should be noted that, in principle, the canting could also be due to the competition of strong single-ion anisotropies of distinct magnetic sublattices. However, this picture would not be compatible with the above weak coercitive fields observed in Fig. 9. No spontaneous moment could be detected in the neutron-diffraction experiment and a simple collinear AFM structure is consistent with this experiment. We can argue that the discrepancy between neutron diffraction and SQUID magnetization experiments is due to the lower sensitivity of the former to the small difference between collinear and canted structures.

A single-crystal study would be required in order to single out separate contributions of the magnetic anisotropy and of the DM mechanism. The hitherto grown crystals are still too small, especially considering the sensitivity limit of the SQUID magnetometer. Nevertheless, we could obtain a hint as to the two contributions and as to the distinct response of the two magnetic sublattices thanks to a series of $M(H)$ measurements carried out according to the following procedure. The $M(H)$ data were taken at selected temperatures after warming above $T_{N,B}$ and cooling down in zero applied field. This procedure ensures that the field is applied when the sample is in a fully demagnetized state. The fraction of spontaneous moment oriented at low field increases upon cooling. The results of these measurements are shown in Fig. 10. We note that all the $M(H)$ curves show a linear behavior at high fields. This response is well known for a classic antiferromagnet and consistent with a superposition of the responses of the two magnetic structures associated with the B and A' sublattices. Such linear response at high field rules out the possibility that the magnetocrystalline anisotropy dominates and we conclude that the contribution of the DM interaction is important to account for the remanence experimentally observed. Note that the DM interaction can be nonzero only for the B ions thanks to the octahedral buckling while it must vanish by symmetry for the A' ions. The lack of DM interaction for the latter is consistent with the pure AFM behavior observed below the ordering transition at $T_{N,A'}$ (see Fig. 8). We finally note that the initial curvature in the low-field region can be explained by extrinsic factors, such as domain-wall motion or local demagnetizing fields, while the initial point of the first magnetization curves of Fig. 10 corresponds to a small nonzero moment because of the residual magnetic field of the superconducting magnet during the ZFC cooling step.

3. Electrical resistivity

As to the transport properties of $LaMn_7O_{12}$, we report in Fig. 11 the temperature-dependent resistivity, $\varrho(T)$, curve. The data show an insulating behavior in the whole 300–170 K range measured, as expected from a half-filled e_g band of octahedral Mn^{3+} ions. The value of room-temperature resistivity is found to be $\varrho(290\ \text{K})=36.3\ \Omega$ cm, compared to the $10^4\ \Omega$ cm value reported for $LaMnO_3$ pellets.[10] This large difference may partly be of extrinsic origin, considering the higher density of our $LaMn_7O_{12}$ samples prepared under high pressure. The transport mechanism is thermally activated as shown by the linear dependence of the Arrhenius plot in the inset of Fig. 11. The data fit yields a value of the activation energy $E_a=0.22$ eV, i.e., about four times the value reported for $NaMn_7O_{12}$.[20] The relatively small values of activation energy reported for both compounds may indi-

cate the presence of midgap defect states. A more reliable measure of the gap value shall be given by optical conductivity measurements, which is the object of a forthcoming publication.[30]

IV. DISCUSSION AND CONCLUSIONS

In conclusion, we carried out a detailed neutron diffraction, specific-heat, magnetization, and electrical conductivity study in order to investigate the crystal structure and the magnetic properties of the high-pressure compound $LaMn_7O_{12}$. We showed that $LaMn_7O_{12}$ is to be compared to the prototype system $LaMnO_3$ because both compounds share a similar pseudocubic perovskitelike structure and the same single-valent Mn^{3+} characteristics. However, $LaMn_7O_{12}$ displays some fundamental structural differences inherent to its high-density *quadruple* perovskite structure stabilized by high pressure. The two salient differences are the much larger Mn-O-Mn buckling angle and the presence of two inequivalent octahedral Mn^{3+} sites. Both features arise from the stabilization of a high-density body-centered $I/2m$ symmetry different from the primitive *Pnma* symmetry of $LaMnO_3$. While the different buckling angle is expected to affect the relevant parameters of the magnetic superexchange interaction, the inequivalent sites lead to different JT distortions of the octahedral Mn^{3+} ions. Our main point is that the combination of these two features should account for the *C*-type AFM structure of the *B* sublattice found at low temperatures in $LaMn_7O_{12}$, which differs from the *A*-type structure characteristic of $LaMnO_3$ and related single-valent $RMnO_3$ compounds. Also, the ordering temperature, $T_{N,B}$, of the Mn^{3+} ions found in $LaMn_7O_{12}$ is at odds with the well-established dependence of T_N on ϕ reported for the $RMnO_3$ system.[11] This suggests that the difference in superexchange parameters, presumably caused by the larger octahedral buckling, is not sufficient to account for the different magnetic structure. Thus, the existence of distinct JT *B* sites seems to play a primary role in the competition between *A*-type and *C*-type structures. In conclusion, $LaMn_7O_{12}$ appears to be a model system for widening our current understanding of the complex magnetic and orbital orderings in perovskitelike e_g Jahn-Teller systems. Current models could be extended to the case of arbitrary values of Mn-O-Mn bond angles and of different JT distortion patterns. For instance, the present magnetization data suggest that the larger buckling of the MnO_6 octahedra increases the strength of the DM interaction, thus increasing the canting of the AFM structure of the *B* sublattice. This large octahedral buckling corresponds to an intermediate situation between the two extreme cases of perpendicular or parallel e_g orbitals in adjacent Mn sites usually considered to account for the FM or AFM exchange interaction within the GKA rule frame. Our observation of thermally activated insulating behavior in $LaMn_7O_{12}$, similar to that found in the $RMnO_3$ system, confirms that a generalized theory of the magnetic and orbital orderings in single-valent systems should be restricted to the case of magnetic superexchange interaction, in agreement with the current view that the double-exchange mechanism is relevant only in mixed-valent or disordered systems.[31] Finally, similarly to the case of the isostructural mixed-valent compound $NaMn_7O_{12}$,[20] also $LaMn_7O_{12}$ is found to display an additional magnetic ordering of the A' ions. This ordering seems to occur independently of that of the *B* ions, which is also similar to the case of $NaMn_7O_{12}$. We believe that this additional magnetic structure offers an opportunity for generalizing the current model of spin and orbital orderings of Jahn-Teller ions. Indeed, the A' sublattice is characterized by a square-planar topology of the magnetic ions, different from that of the *B* sublattice. This is expected to lead to different *t* and *U* superexchange parameters, and to a different symmetry of the electronic states, which may explain the lack of sizable interaction between the two magnetic sublattices.

ACKNOWLEDGMENTS

We thank G. Calestani, R. De Renzi, A. Daoud-Aladine, S. Lupi, and G. Rousse for helpful discussions. A.P. acknowledges financial support from the "Fondazione A. Della Riccia." E.G. acknowledges support from the Short Mobility Program of the Consiglio Nazionale delle Ricerche (CNR), Italy. Part of the high-pressure synthesis work was carried out at the Bayerisches Geoinstitut of Bayreuth, Germany, in the framework of the European Transnational Access to Infrastructures Program.

*Corresponding author; andrea.gauzzi@upmc.fr

[1] E. O. Wollan and W. C. Koehler, Phys. Rev. **100**, 545 (1955).
[2] Y. Tokura and N. Nagaosa, Science **288**, 462 (2000).
[3] Y. Tokura Ed, *Colossal Magnetoresistive Oxides* (Gordon and Breach Science, New York, 2000).
[4] J. B. Goodenough, *Magnetism and Chemical Bond* (Interscience, New York, 1963).
[5] P. W. Anderson, Phys. Rev. **115**, 2 (1959).
[6] J. Kanamori, J. Phys. Chem. Solids **10**, 87 (1959).
[7] P. W. Anderson, in *Solid State Physics*, edited by F. Seits and D. Tumbull (Academic, New York, 1963), Vol. 14, p. 99.
[8] E. F. Bertaut, Acta Crystallogr., Sect. A: Cryst. Phys., Diffr., Theor. Gen. Crystallogr. **24**, 217 (1968).
[9] J. Rodriguez-Carvajal, M. Hennion, F. Moussa, A. H. Moudden, L. Pinsard, and A. Revcolevschi, Phys. Rev. B **57**, R3189 (1998).
[10] B. Dabrowski, S. Kolesnik, A. Baszczuk, O. Chmaissem, T. Maxwell, and J. Mais, J. Solid State Chem. **178**, 629 (2005).
[11] J. S. Zhou and J. B. Goodenough, Phys. Rev. B **68**, 054403 (2003).
[12] M. Marezio, P. D. Dernier, J. Chenavas, and J. C. Joubert, J. Solid State Chem. **6**, 16 (1973).
[13] B. Bochu, J. Chenavas, J. C. Joubert, and M. Marezio, J. Solid State Chem. **11**, 88 (1974).
[14] A. Deschanvres, B. Raveau, and F. Tollemer, Bull. Soc. Chim. Fr., Issue 11, 4077 (1967).

[15] B. Bochu, J. C. Joubert, A. Collomb, B. Ferrand, and D. Samaras, J. Magn. Magn. Mater. **15-18**, 1319 (1980).
[16] A. Larson and R. von Dreele, Los Alamos National Laboratory Report LAUR 86-748, 2000.
[17] D. I. Khomskii and K. I. Kugel, Solid State Commun. **13**, 763 (1973).
[18] It is recalled that $I2/m$ is the short-hand notation for the space-group No. 12 $C2/m$ with unique axis b and cell choice 3. See also *International Tables of Crystallography*, edited by Th. Hahn (Kluwer Academic, London, 1989), Vol. A.
[19] I. Solovyev, N. Hamada, and K. Terakura, Phys. Rev. Lett. **76**, 4825 (1996).
[20] A. Prodi, E. Gilioli, A. Gauzzi, F. Licci, M. Marezio, F. Bolzoni, Q. Huang, A. Santoro, and J. W. Lynn, Nature Mater. **3**, 48 (2004).
[21] A. Prodi, G. Allodi, E. Gilioli, F. Licci, M. Marezio, F. Bolzoni, A. Gauzzi, and R. De Renzi, Physica B **374-375**, 55 (2006).
[22] A. Gauzzi, E. Gilioli, A. Prodi, F. Bolzoni, F. Licci, M. Marezio, G. Calestani, M. Affronte, Q. Huang, and A. Santoro, J. Supercond. **18**, 675 (2005).
[23] B. C. Hauback, H. Fiellvåg, and N. Sakai, J. Solid State Chem. **124**, 43 (1996).
[24] J. Topfer and J. B. Goodenough, J. Solid State Chem. **130**, 117 (1997).
[25] I. Dzyaloshinsky, J. Phys. Chem. Solids **4**, 241 (1958).
[26] T. Moriya, Phys. Rev. **120**, 91 (1960).
[27] R. M. Bozorth, Phys. Rev. Lett. **1**, 362 (1958).
[28] V. Skumryev, F. Ott, J. M. D. Coey, A. Anane, J. P. Renard, L. Pinsard-Gaudard, and A. Revcolevschi, Eur. Phys. J. B **11**, 401 (1999).
[29] F. Bolzoni and R. Cabassi, J. Appl. Phys. **103**, 063905 (2008).
[30] S. Lupi *et al.* (private communication).
[31] J. B. Goodenough, Phys. Rev. **100**, 564 (1955).